Effects of magnetic ordering on dynamical conductivity: optical investigations of EuFe2As2 single crystals

D. Wu, N. Barišić, N. Drichko, S. Kaiser, A. Faridian, M. Dressel, S. Jiang, Z. Ren, L. J. Li, G. H. Cao, Z. A. Xu, H. S. Jeevan, Philipp Gegenwart

Angaben zur Veröffentlichung / Publication details:

Wu, D., N. Barišić, N. Drichko, S. Kaiser, A. Faridian, M. Dressel, S. Jiang, et al. 2009. "Effects of magnetic ordering on dynamical conductivity: optical investigations of EuFe2As2 single crystals." *Physical Review B* 79 (15): 155103. https://doi.org/10.1103/physrevb.79.155103.

Effects of magnetic ordering on dynamical conductivity: Optical investigations of $EuFe_2As_2$ single crystals

D. Wu,* N. Barišić, N. Drichko, S. Kaiser, A. Faridian, and M. Dressel
Physikalisches Institut, Universität Stuttgart, Pfaffenwaldring 57, 70550 Stuttgart, Germany

S. Jiang, Z. Ren, L. J. Li, G. H. Cao, and Z. A. Xu
Department of Physics, Zhejiang University, Hangzhou 310027, People's Republic of China

H. S. Jeevan and P. Gegenwart
I. Physikalisches Institut, Georg-August-Universität Göttingen, 37077 Göttingen, Germany
(Received 3 March 2009; revised manuscript received 11 March 2009; published 7 April 2009)

The magnetic, transport, and optical properties of $EuFe_2As_2$ single crystals have been investigated parallel and perpendicular to the *ab* plane. The anisotropy $\rho_c/\rho_{ab} \approx 8$ depends only slightly on temperature. In both orientations, the spin-density-wave transition at $T_{SDW}=189$ K shows up as a considerable increase in the dc resistivity. Susceptibility measurements evidence the magnetic order of the Eu^{2+} moments at $T_N=19$ K with little influence on the electronic transport taking place in the FeAs layers. Polarization-dependent infrared spectroscopy reveals strongly anisotropic optical properties and yields a carrier density of only 4.2×10^{21} cm^{-3} and a bandmass of $m_b=2m_0$. A sizeable Drude contribution is present at all temperatures and narrows upon cooling. Below T_{SDW}, the spin-density-wave gap develops in the in-plane optical conductivity; no appreciable change is detected for the perpendicular polarization. Modifications in the phonon features are associated with changes in the electronic properties at T_{SDW}. The extended Drude analysis yields a linear behavior of the frequency-dependent scattering rate below T_{SDW}, indicating an interaction between the charge carriers and spin fluctuations in the spin-density-wave state.

DOI: 10.1103/PhysRevB.79.155103 PACS number(s): 75.30.Fv, 75.20.Hr, 78.20.Ci

I. INTRODUCTION

There are a small number of fundamental issues in solid-state science that remain of central importance even when a new class of materials emerges. Besides the effect of reduced dimensions and the Mott transition, the interplay of magnetism and superconductivity is certainly among those fascinating topics. It has been intensively explored in heavy-fermion compounds,[1] organic conductors,[2] and cuprates;[3] all of them exhibit certain types of magnetic order in the close vicinity to a superconducting phase of unconventional nature.

The observation of $T_c=26$ K superconductivity in $LaFeAsO_{1-x}F_x$ has brought a new round of investigations since iron is supposed to form magnetic order at low temperature. Two classes of ferropnictide superconductors have drawn extensive attention, i.e., doping of *Ln*FeAsO (*Ln* =lanthanides) and AFe_2As_2 (A=Sr, Ba, etc.) by holes or electrons. The parent compounds of these two systems are suggested to have a spin-density-wave (SDW) instability associated with the FeAs layers in the temperature range between 130 and 200 K that will be gradually suppressed upon charge-carrier doping, and finally the material becomes superconducting.[4–7] By now the relation of the antiferromagnetic spin fluctuations to the mechanism of superconductivity is not clear. Around T_{SDW} also a structural transition is observed, where the symmetry changes from tetragonal ($I4/mmm$) to orthorhombic ($Fmmm$).[8]

Like in $BaFe_2As_2$ and $SrFe_2As_2$, Mößbauer spectroscopy and magnetic susceptibility studies of $EuFe_2As_2$ revealed[9,10] the magnetic transition due to an antiferromagnetic (AFM) ordering of itinerant carriers in the Fe sublattice that form a SDW; in the title compound the temperature of the phase transition is approximately 190 K. The peak in resistivity $\rho(T)$ supports this assignment; however, the relation to the structural transition around the same temperature is not solved by now. Compared with other compounds of the AFe_2As_2 family, the exceptional case in $EuFe_2As_2$ is that in coexistence to the SDW phase a second magnetic ordering takes place in the localized Eu moments at $T_N=19$ K.[10]

While in $BaFe_2As_2$ Co or Ni substitution of Fe causes a suppression of the SDW and the appearance of a superconducting state.[11,12] No superconductivity is found in the Eu analog $EuFe_{2-x}Ni_xAs_2$;[13] nevertheless, there seems to be some interaction between the Eu and Fe/Co/Ni subsystems, because the arrangement of the Eu moments turns to be ferromagnetic for $x>0.06$.[13] Replacing Eu by K, for instance, suppresses the SDW, and also substantially broadens the Eu order and shifts it down below 10 K; in spite of the short-range magnetic order, at $T_c=31$ K superconductivity is detected in $Eu_{0.5}K_{0.5}Fe_2As_2$.[14,15]

Applying pressure to $EuFe_2As_2$ suppresses the SDW phase, too, but only some onset of superconductivity was inferred at $T_c \approx 29.5$ K where a drop in resistivity is detected above 2 GPa (Ref. 16); the AFM ordering temperature of the Eu^{2+} moments is nearly unaffected by pressure. Very recently, superconductivity was reported in $EuFe_2As_2$ by partially substituting As by isovalent P, inducing chemical pressure without destroying the magnetic transition of the Eu^{2+} moments.[17] This agrees with predictions of magnetic quantum criticality between an antiferromagnetic and paramagnetic metal.[18] As a matter of fact, the ferromagnetic interaction between the Eu^{2+} moments (which is probably due to

RKKY interaction) is strengthened as a consequence of P doping in a similar manner as observed in $EuFe_{2-x}Ni_xAs_2$. Here we investigate the influence of these different magnetic ordering phenomena on the charge-carrier dynamics in $EuFe_2As_2$ in order to elucidate the effect of spin fluctuations on the superconducting ground state in ferropnictides, in general.

II. EXPERIMENTAL DETAILS

Single crystals of $EuFe_2As_2$ were grown using FeAs as self-flux dopants.[10] The platelets with a typical size of 4 mm×2 mm×0.5 mm have naturally flat surface. The specimens from two different laboratories were characterized by transport and susceptibility measurements; the good agreement obtained in all results confirms the intrinsic nature of the findings reported here. The temperature-dependent dc resistivity was obtained by standard four-probe technique using silver paint as contacts. For the out-of-plane measurements, the mechanic stability of the contacts during temperature sweeps and interlayer inclusions of presumably unreacted precursor material cause severe problems. Therefore particular care has to be taken to obtain quantitatively reproducible results.[19] The magnetic susceptibility was measured down to 4 K by a Quantum Design superconducting quantum interference device system at different magnetic fields up to 2 T applied parallel and perpendicular to the *ab* plane.[20]

The optical reflectivity was investigated by Fourier transform spectroscopy with the electric field polarized in both the *ab* plane and the *c* direction. The Bruker IFS 113v and IFS 66v/s interferometers utilized in our study cover the frequency range from 30 to 12 000 cm^{-1}. The experiments were performed at various temperatures down to 10 K. As reference, gold was evaporated onto the sample *in situ* and the measurements repeated at each temperature. The *c*-axis infrared experiments were performed using an infrared microscope Bruker Hyperion. For the high-frequency extrapolation up to the ultraviolet, we used room-temperature ellipsometric data (6000–30 000 cm^{-1}) by a Woollam variable angle spectroscopic ellipsometer. The low-frequency extrapolation was done according to the dc conductivity. The complex optical conductivity $\hat{\sigma}(\omega)=\sigma_1(\omega)+i\sigma_2(\omega)$ was calculated from the reflectivity spectra using Kramers-Kronig analysis.[21] It is worth to note, that we also applied a simple Hagen-Rubens extrapolation for the low-frequency reflectivity in $E\|ab$ polarization, and found that the optical conductivity in the measured range does not depend on the extrapolation. In the perpendicular direction, we extrapolated by assuming a constant reflectivity.

In addition, we have performed far-infrared reflection measurements in an optical cryostat Oxford Spectromag 4000 where a magnetic field up to 5 T can be applied perpendicular to the *ab* plane. The experiments were performed down to $T=2$ K with particular emphasis on the magnetic ordering at $T_N=19$ K.

III. RESULTS

A. Electrical resistivity

$EuFe_2As_2$ is a poor metal with a room-temperature conductivity of only 2.5×10^3 $(\Omega\ cm)^{-1}$ which is more than 2 orders of magnitude lower compared to normal metals such as iron or gold. From the analysis of our optical data discussed below in Sec. IV A, we conclude that this is mainly due to the reduced charge-carrier density. The electrical resistivity of several $EuFe_2As_2$ crystals was measured in the *ab* plane and in *c* direction. The results are plotted in Fig. 1 as a function of temperature. When T is reduced below room temperature, the in-plane resistivity slowly decreases as $\rho_{ab}\propto T$. This is similar to the behavior reported for high-T_c cuprates above T^*. A peak in ρ_{ab} is observed at $T_{SDW}\approx189$ K associated with the SDW transition. The rise in resistivity evidences the loss in density of states at the Fermi energy upon entering the SDW phase. A similar peak is observed in the perpendicular direction, $\rho_c(T)$, indicating that the gap opens more or less isotropically over the entire Fermi surface. However, the resistivity soon continues to drop as the temperature is reduced further; this means that not all bands are affected by the SDW transition. Our conclusions are in accord with previous findings.[13,14,22–25]

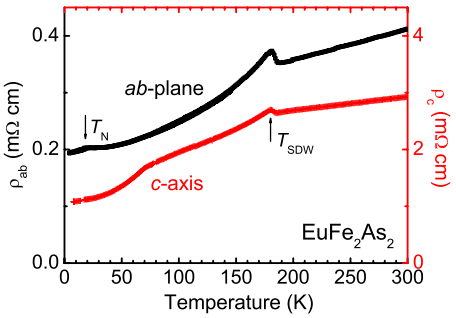

FIG. 1. (Color online) Temperature dependence of resistivity ρ_{ab} (black squares, left axis) in the *ab* plane and ρ_c (red crosses, right axis) in the perpendicular direction of single crystalline $EuFe_2As_2$. The spin-density-wave transition T_{SDW} and the antiferromagnetic order of Eu at T_N are indicated by arrows.

Compared to the linear resistivity behavior above T_{SDW}, which might be influenced by fluctuations of the Fe spins, the slope of $\rho(T)$ curve gets even steeper for $T<T_{SDW}$, because the scattering rate of carriers is reduced in the SDW state, where some of the bands become (partially) gapped. Here the in-plane resistivity follows a quadratic temperature dependence $\rho(T)\propto T^2$ all the way down to 30 K where it saturates at a constant value. It seems unlikely that this behavior is due to electron-electron scattering but might express scattering on magnetic excitations where a T^2 behavior is predicted for a ferromagnet and T^4 for an antiferromagnet,[26] with details strongly depending on the dispersion relation.

At $T_N=19$ K we observe a kink in $\rho_{ab}(T)$ because another scattering channel freezes out due to the AFM ordering of the Eu^{2+} moments. Obviously, the energy scales of the SDW linked to Fe and the AFM order in the Eu sublattice are different by an order of magnitude, as indicated by the ordering temperature. The two phase transitions also influence the electronic scattering very differently: for $T<T_{SDW}$ the scattering is strongly reduced, while the change at T_N is minor.

The resistivity measured along the perpendicular direction exceeds ρ_{ab} considerably: $\rho_c(300\ K)=3\ m\ \Omega\ cm$.[19] Never-

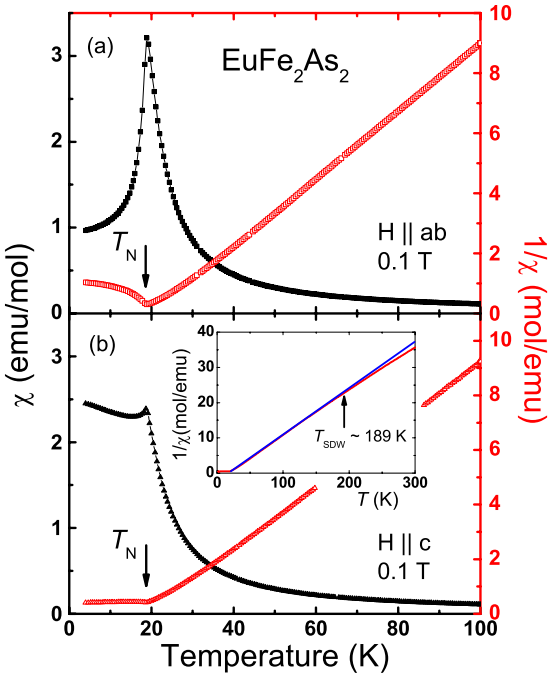

FIG. 2. (Color online) Magnetic susceptibility of $EuFe_2As_2$ for (a) the *ab* plane and (b) the *c* direction from $T=2$ K to 100 K (left axes). Corresponding to the right axes the inverse susceptibility $1/\chi$ is plotted for both orientations. The inset shows the inverse susceptibility after subtracting the temperature-independent terms for $H\|c$ (red curve) in a wider temperature range (2 K$<T<$300 K) (Ref. 10); the blue line indicates the Curie-Weiss fit up to 300 K. $1/\chi_{ab}$ (not shown) has the same trend as χ_c above 200 K.

theless, the temperature behavior $\rho_c(T)$ closely resembles the in-plane properties; the anisotropy ratio $\rho_c/\rho_{ab}\approx 8$ is almost temperature independent. Hence, $EuFe_2As_2$ exhibits a metallic behavior of $\rho(T)$ in both directions. Although the two-dimensional layered structure is identified for the FeAs-based compounds as in cuprates, this observation is distinct from high-T_c cuprates which commonly exhibit different temperature dependences of the in-plane and out-of-plane resistivity.[27] Our findings, of only weak anisotropic in dc conductivity, support the conclusion of high-magnetic-field measurements[28,29] indicating nearly isotropic superconductivity in $(Ba,K)Fe_2As_2$.

The SDW of the Fe ions can clearly be seen in $\rho_c(T)$ indicating its three-dimensional nature. Similar observations have been reported for the sister compound $BaFe_2As_2$.[30] The AFM transition at $T_N=19$ K is not seen in $\rho_c(T)$, in contrast to the in-plane resistivity. This is somewhat surprising and infers that the magnetic order of Eu^{2+} ions does not lead to a complete three-dimensional arrangement. Albeit long-range order is established in plane, it might be only short range in the perpendicular direction.

B. Magnetic susceptibility

Figure 2 exhibits the temperature dependence of the magnetic susceptibility $\chi(T)$ of $EuFe_2As_2$ measured for a magnetic field of 0.1 T oriented both parallel and perpendicular to the *ab* plane. Also shown is the inverse susceptibility

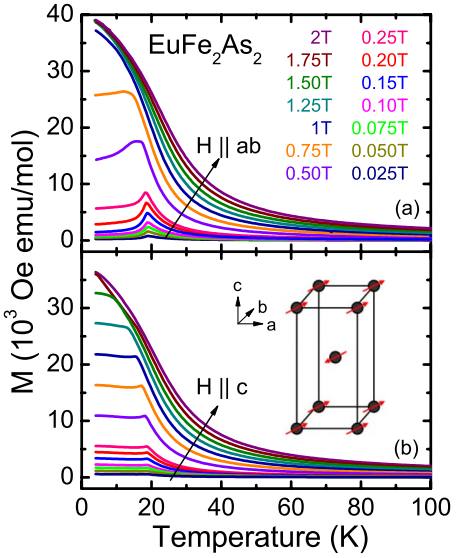

FIG. 3. (Color online) Temperature dependence of the magnetization of $EuFe_2As_2$ under various fields up to 2 T; the development with magnetic field strength is indicated by the arrows. For both orientations, M_{ab} and M_c continuously increase with rising magnetic field H, as indicated by the black arrows. The inset shows a schematic diagram for the Eu magnetic structure. The long axis represents the *c* axis; the red arrows indicate the spins of Eu which are not completely within the *ab* plane.

$1/\chi_{ab}(T)$ and $1/\chi_c(T)$ which clearly proves that the paramagnetic regime can be nicely described by the Curie-Weiss law. As demonstrated in the inset of Fig. 2, this behavior is well observed over a very wide temperature range from 20 to 200 K; here the magnetic response is isotropic. Slight deviations from $\chi(T)\propto 1/T$ are only observed for higher temperatures, i.e., above the SDW transition which is identified as a tiny kink.

At $T_N=19$ K, a distinct anomaly shows up in both orientations that is ascribed to the ordering of the Eu^{2+} moments.[10] It is concluded that the Eu^{2+} spins align ferromagnetically within the *ab* planes, but antiferromagnetically along the *c* direction, as sketched in the inset of Fig. 3. The upturn of $\chi_c(T)$ below $T=18$ K indicates a metamagnetic transition of Eu in this direction.[10,31] The excellent quality of our samples is confirmed by the good agreement of our results with the report by Jiang *et al.*,[10] where also a more detailed description of $\chi(T)$ can be found. It should be noted that although Fe and Eu both carry magnetic moments, which is a unique behavior in AFe_2As_2 family, there is almost no coupling between both subsystems; one reason is the large difference of energy scales for local Eu ordering and itinerant Fe antiferromagnetism. Nevertheless, the resistivity behavior and magnetoresistance studied in Ref. 10 reflect that the charge carriers are scattered by the Eu moments to some degree. In addition, the absence of superconductivity in $EuFe_{2-x}Ni_xAs_2$—while it is present in Ni doped $BaFe_2As_2$—indicates that the magnetic state of Eu affects superconductivity.[13] In the same direction goes the conclusion drawn from the Eu substitution by K.[14,15]

Further investigations of the magnetization $M_{ab}(T)$ and $M_c(T)$ under various magnetic fields are presented in Fig. 3.

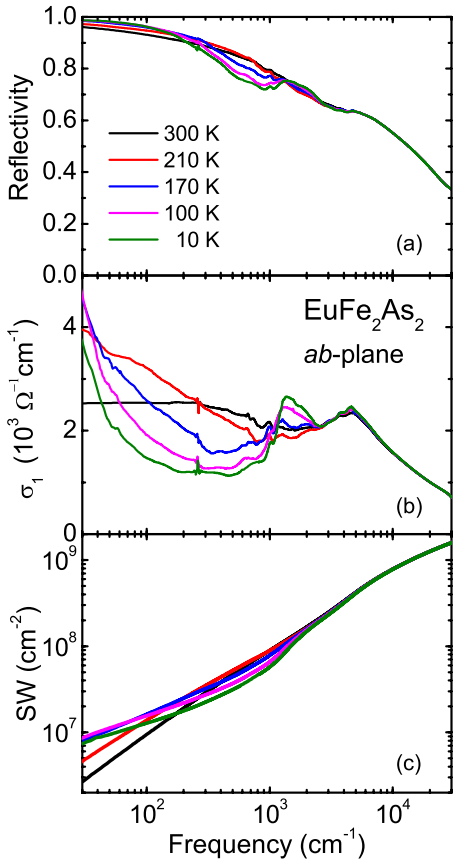

FIG. 4. (Color online) Optical properties of $EuFe_2As_2$ in the *ab* plane measured in a broad frequency range at different temperatures. (a) The reflectivity $R(\omega)$ drops around 1250 cm^{-1} for $T=170$ K and lower since the SDW state is entered at $T_{SDW}=189$ K. (b) The corresponding optical conductivity indicates the development of the SDW gap around 1000 cm^{-1}; nevertheless there remains a strong background of excitations in the gap. (c) The spectral weight calculated according to Eq. (1) is displayed in a double-logarithmic fashion.

With increasing field up to 0.75 T, the AFM transition in *ab* plane gradually shifts to lower temperature. For $\mu_0 H \geq 1$ T, the metamagnetic transition is suppressed, and $M_{ab}(T)$ tends to saturate below 10 K, indicating a full ferromagnetic state of the Eu moments. In the case of $H \| c$, a significantly higher external magnetic field ($\mu_0 H > 1.5$ T) is needed to fully suppress the AFM ordering of Eu [Fig. 3(b)]. This suggests that the Eu moments align close to the *ab* plane but still have a *c*-axis component [cf. the schematic diagram in Fig. 3(b)].

C. Optical properties

The upper panel of Fig. 4 shows the *ab*-plane reflectivity $R(\omega)$ in the whole spectral range for some selected temperatures as indicated. Above $T \approx 200$ K the reflectance resembles a metal, although the plasma edge is not clearly seen; a fact well known from high-temperature and organic superconductors.[32,33] This expresses the poor metallic behavior, already seen in resistivity (Sec. III A); but also the overlap with interband transitions leads to an overdamped plasma edge. At 1000 cm^{-1} the reflectance is already as low as 80%.

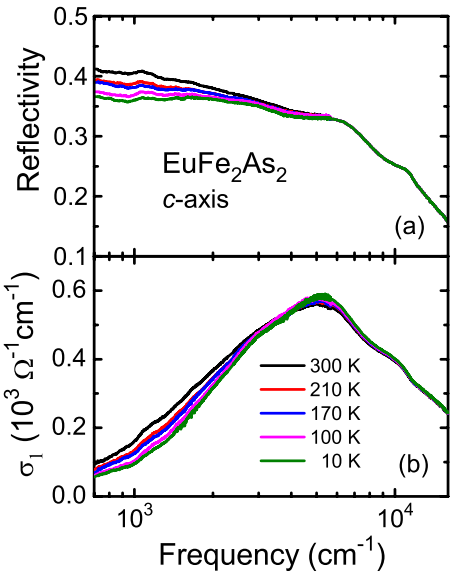

FIG. 5. (Color online) Optical properties of $EuFe_2As_2$ measured at various temperatures with the electric field *E* polarized in the *c* direction. (a) The mid-infrared reflectivity is much lower compared to the *ab*-plane reflectance and decreases even further when the temperature is reduced. (b) The optical conductivity is dominated by the mid-infrared band around 5000 cm^{-1} ascribed to an interband transition.

Below the SDW transition, $T_{SDW}=189$ K, a drop in $R(\omega)$ is observed around 1250 cm^{-1} that is fully developed when *T* reaches 10 K. The reflectivity is strongly suppressed between 200 and 1000 cm^{-1}; but it rapidly increases toward unity for $\omega \to 0$ because the compound remains metallic for any temperature.

For all temperatures the in-plane optical conductivity spectra $\sigma_1(\omega,T)$ of $EuFe_2As_2$ show a broad peak in the mid-infrared (5000 cm^{-1}) due to interband transitions [Fig. 4(b)].[23] This maximum gets slightly stronger as the temperature is reduced, basically recovering the spectral weight lost in the low-frequency region (see below). For $T < T_{SDW}$, the frequency region below 1000 cm^{-1} is depleted and the spectral weight piles up around 1300 cm^{-1}. Although the Drude contribution is appreciably reduced, it is always present, indicating a partial gap opening of the Fermi surface. The zero-frequency peak narrows upon cooling because of the decreasing scattering rate of the charge carriers. This is in accord with the observation from a falling dc resistivity (Fig. 1).

In the *c* direction (Fig. 5), the $R(\omega)$ shows only 40% reflectance in the mid-infrared and gradually falls at high frequencies. On lowering the temperature, $R(T)$ decreases by not more than 10%. The optical conductivity exhibits a broad maximum around 5000 cm^{-1} which only slightly varies with temperature; it corresponds to the same interband transition detected in the *ab* plane. Although $\sigma_1(T)$ is reduced by a factor of 2 in the range of 1000 cm^{-1}, when going from room temperature to 10 K, the indications of a SDW gap are not as clear as for the in-plane conductivity. Considerable changes are already seen for $T > 200$ K and the variation extends all the way up to 3000 cm^{-1}, i.e., well above the

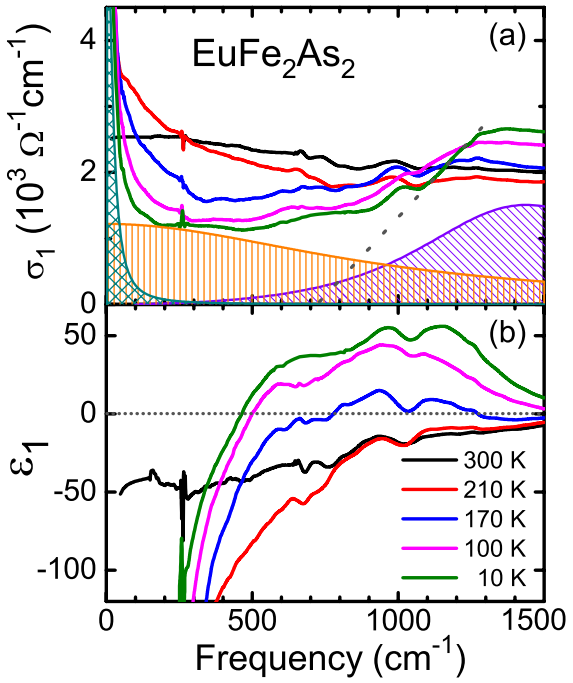

FIG. 6. (Color online) Low-frequency optical properties (up to 1500 cm^{-1}) of $EuFe_2As_2$ at various temperatures for $E\|ab$. (a) The optical conductivity can be decomposed in two Drude-type contributions (olive pattern and orange shaded), and an oscillator to mimic the SDW gap (violet shaded), as depicted for the 10 K data for instance. (b) The frequency dependence of the dielectric constant exhibits a zero crossing ($d\epsilon_1/d\omega>0$) as low as 500 cm^{-1}.

energy identified as the SDW gap by the in-plane measurements. Thus we conclude that the formation of the SDW state is not observed in the optical properties for $E\|c$ in spite of the clear feature present in the dc resistivity $\rho_c(T)$. In general, the substantial difference in the optical properties of polarization $E\|c$ compared to the in-plane results is in compliance with the dc anisotropy ratio of 10, although we could not see indications of a Drude-like peak in our limited frequency range.

IV. ANALYSIS AND DISCUSSION

A. Charge-carrier density

As a first step, we fit the conductivity spectra of $EuFe_2As_2$ by the Drude-Lorentz model;[21] this allows us to separate different contributions. As an example, in Fig. 6(a) the terms are plotted for the low-temperature data $\sigma_1(\omega, T=10\ \mathrm{K})$. If the conductivity peak around 5000 cm^{-1} is modeled by a Lorentz term and ascribed to an interband transition, the quasi-free-carrier parts remaining at lower frequencies yield a plasma frequency of approximately 14 000 cm^{-1} at room temperature. This value for $EuFe_2As_2$ is in good agreement with $\omega_p/2\pi c \approx 12\ 000\ cm^{-1}$ obtained in the sister compounds $BaFe_2As_2$ and $SrFe_2As_2$.[34]

Alternatively, we can calculate the spectral weight[21]

$$\mathrm{SW}(\omega_c) = 8\int_0^{\omega_c} \sigma_1(\omega)d\omega = \omega_p^2 = \frac{4\pi n e^2}{m} \qquad (1)$$

as a function of cut-off frequency ω_c. As seen in Fig. 4(c), no obvious step or saturation evidences a plasma frequency up to 30 000 cm^{-1}; this is in accord with the gradual decrease in the reflectivity $R(\omega)$ to higher frequencies [Fig. 4(a)]. Although the spectral weight shifts to higher frequencies below the SDW transition, it is basically recovered around 2500 cm^{-1} as can be seen from the merger of the different curves in Fig. 4(c). Hence, the overall spectral weight remains conserved at any temperature. The same behavior was observed in optical experiments of the Ba and Sr analogues.[34,35] To leave out the interband transition at 5000 cm^{-1} and consider only the itinerant electrons, we have chosen $\omega_c/2\pi c = 2500\ cm^{-1}$ as suitable cut-off frequency and then get 13 800 cm^{-1} for the quasi-free-carrier plasma frequency.

Using Eq. (1) with $m=2m_0$ the bandmass—as obtained from our extended Drude analysis discussed below in Sec. IV D—and $\omega_p/2\pi c \approx 13\ 800\ cm^{-1}$, the carrier density is estimated to be $n \approx 4.2\times10^{21}\ cm^{-3}$, significantly lower than typical for conventional metals. If we convert n to the number of carriers N per unit cell by using the low-temperature volume $V_{\mathrm{cell}}=0.3683\ nm^3$ for $Z=4$ reported by Tegel *et al.*,[36] we obtain $N \approx 0.39$ electrons per formula unit.

B. Spin-density-wave gap

Upon passing through the SDW transition, there is a strong reduction in the optical conductivity below 1200 cm^{-1} as magnified in the linear-frequency presentation of Fig. 6(a). With decreasing temperature the peak above the SDW gap grows and also the gap becomes slightly larger, as expected from a mean-field transition. From a linear extrapolation of the 10 K conductivity (dotted line), we can estimate a gap value of $2\Delta_0 \approx 750\ cm^{-1}$, well above the mean-field value of $2\Delta_0 = 3.53T_{\mathrm{SDW}} \approx 470\ cm^{-1}$. In $SrFe_2As_2$ ($T_{\mathrm{SDW}} \approx 200$ K) Hu *et al.*[34] identified two gaps with peaks at 500 and 1500 cm^{-1}; accordingly for $BaFe_2As_2$ ($T_{\mathrm{SDW}}=138$ K) they find the double peak features at lower energies (360 cm^{-1} and 890 cm^{-1}). The Eu compound investigated in the present study falls right between with $T_{\mathrm{SDW}}=189$ K, and the 1300 cm^{-1} maximum is likely to correspond to the reported high-frequency peak. However, we cannot find clear indications for a low-energy gap. Around 600 cm^{-1}, a small step might be identified, in particular in the 100 K spectrum, but since it smears out upon lowering the temperature instead of getting more pronounced, we hesitate to associate it with a second gap. Also the dielectric constant shown in Fig. 6(b) gives no evidence for a two-gap structure. Interestingly, for $BaFe_2As_2$ Pfuner *et al.*[35] reported a pseudogap of 500 cm^{-1}, but they did not observe changes at higher energies, in contrast to Hu *et al.*[34,37] Multiple-gap features are not surprising for a compound with many bands crossing the Fermi energy; similar properties have been reported in MgB_2,[38] the model compound of a two-gap superconductor.

To estimate the spectral-weight shift upon opening of the SDW gap, we identify an isobetic point $\omega_i \approx 1050\ cm^{-1}$ in the optical spectra below which $\sigma_1(\omega)$ decreases as $T < T_{\mathrm{SDW}}$ and above which the spectral weight piles up. As can be seen in Figs. 4(b) and 6(a), $\sigma_1(\omega_i)$ basically remains unaltered with temperature. The relative shift in spectral weight

$$\Delta\mathrm{SW} = \frac{\mathrm{SW}(\omega_i, T=300\ \mathrm{K}) - \mathrm{SW}(\omega_i, T=10\ \mathrm{K})}{\mathrm{SW}(\omega_i, T=300\ \mathrm{K})} \qquad (2)$$

is approximately 35%.

Supplementary information can be obtained from the dielectric constant $\epsilon_1(\omega)=1-4\pi\sigma_2(\omega)/\omega$ plotted in Fig. 6(b). The zero crossing of $\epsilon_1(\omega)$ at $\omega_0/2\pi c=1270$, 1600 and 1780 cm^{-1}, for $T=170$, 100 and 10 K, respectively, is an alternative method to identify the SDW gap.

At all temperatures, there remains some zero-frequency contribution that pulls the dielectric constant negative as expected for a metal. For low temperatures, the zero crossing with positive slope ($d\epsilon_1/d\omega>0$) occurs around $\tilde{\omega}_p/2\pi c=\omega_{p,D}/\sqrt{\epsilon_1}\approx 460$ cm^{-1}, where $\tilde{\omega}_p$ denotes the screened plasma frequency of the zero-frequency contribution which shifts only little for $T\leq 100$ K. From Fig. 6(b) we see that the dielectric constant reaches $\epsilon_1\approx 55$ for $T=10$ K, which yields $\omega_{p,D}/2\pi c\approx 3400$ cm^{-1} for the narrow Drude-like contribution. This value agrees well with the one we get from the Drude-Lorentz fit shown in Fig. 6(a), where the narrow Drude contribution has $\omega_{p,D}/2\pi c=3150$ cm^{-1} at $T=10$ K.

It is apparent from Fig. 6(a) that there exists a sizeable electronic background in the range between 200 and 700 cm^{-1} that stays at all temperatures. While at $T=300$ K this contribution is not so clear, it starts to be well pronounced at $T=210$ K and changes only little below 100 K. It should also be noted that the background conductivity is present in all compounds of this ferropnictide family; for instance, it is seen in the superconducting $Ba_{0.55}K_{0.45}Fe_2As_2$, too, where the magnetic order is suppressed by doping.[39] Hence we do not related this term to the SDW transition. This electronic background could be interpreted as a high-frequency tail of the Drude-like contribution appearing due to interactions of the charge carriers with other excitations. Another possibility would be to describe this feature by a broad Drude term with a width around 1000 cm^{-1} [the orange shaded contribution in Fig. 6(a)]. Since the Fermi level is crossed by five Fe $3d$ bands according to theoretical studies,[22,24] zero-frequency contributions could stretch well above the far-infrared to account for excitations in different Fe $3d$ bands.

C. Magnetic-field dependence

In order to obtain information on the magnetic scattering effects, we have measured the in-plane optical reflectivity in the frequency range 20–700 cm^{-1} when a magnetic field was applied up to 5 T. In the far-infrared (up to 600 cm^{-1}) we find an overall rise of the 10 K reflectivity (not shown). For $\mu_0 H=1$ T it is only 1%, but increases to 5% at 5 T. The reflectivity enhancement with magnetic field diminishes as the temperature increases; above 30 K, no significant change is observed. This infers that the scattering of the remaining conduction electrons described by the broad Drude term in Fig. 6(a) (orange shaded) is partially suppressed by the magnetic field. This behavior does not change upon passing the magnetic order at $T_N=19$ K, which implies that the ferromagnetic order of the Eu moments taking place above 1 T has no appreciable influence on the optical properties in this frequency range.

D. Extended Drude analysis

A deeper insight into the low-energy excitations and the relevant scattering mechanisms of $EuFe_2As_2$ is obtained by performing an extended Drude analysis of the conductivity spectra; here the scattering rate $1/\tau(T,\omega)$ and effective mass $m^*(T,\omega)$ are assumed to be frequency dependent.[21] This approach is commonly applied to correlated electron systems such as heavy fermions, organics, and high-temperature superconductors:[33,40]

$$\hat{\sigma}(\omega)=\frac{\omega_p^2}{4\pi}\frac{1}{\Gamma_1(\omega)-i\omega[m^*(\omega)/m_b]}. \tag{3}$$

Here $\Gamma_1(\omega)$ is the real part of a complex frequency-dependent scattering rate $\hat{\Gamma}(\omega)=\Gamma_1(\omega)+i\Gamma_2(\omega)$, with the imaginary part related to the frequency-dependent mass $m^*/m_b=1-\Gamma_2(\omega)/\omega$ enhanced compared to the bandmass m_b. From the complex conductivity we obtain expressions for $\Gamma_1(\omega)$ and $m^*(\omega)$ in terms of $\sigma_1(\omega)$ and $\sigma_2(\omega)$ as follows:

$$\Gamma_1(\omega)=\frac{\omega_p^2}{4\pi}\frac{\sigma_1(\omega)}{|\hat{\sigma}(\omega)|^2}, \tag{4a}$$

$$\frac{m^*(\omega)}{m_b}=\frac{\omega_p^2}{4\pi}\frac{\sigma_2(\omega)/\omega}{|\hat{\sigma}(\omega)|^2}. \tag{4b}$$

The frequency-dependent scattering rate $1/\tau(\omega)=2\pi c\Gamma_1(\omega)$ and mass $m^*(\omega)$ are plotted in Figs. 7(b) and 7(c) for various temperatures.

It is important to note that the absolute values of $1/\tau$ and m^* strongly depend on the chosen plasma frequency ω_p in Eq. (3); as mentioned above, this is not that clear cut. Nevertheless, the frequency dependence is not influenced by this renormalization and gives the insight into the physics. From the room-temperature spectra, using $\omega_p=13$ 800 cm^{-1}, we can calculate an effective mass by Eq. (1) that corresponds to the optical bandmass $m_b\approx 2m_0$. This is a reasonable value and independent of frequency as expected for a Drude metal. Accordingly, the scattering rate is constant at about $1/\tau\approx 6000$ cm^{-1}. At $T=210$ K we already notice a gradual increase in m^*/m_b down to low energies [Fig. 7(c)]. The corresponding scattering rate slightly increases with frequency due to the shaping up of the narrow zero-frequency response as plotted in Fig. 7.

In the SDW state, some of the electronic bands are gapped, implying that only a reduced number of carriers is available for transport, as seen from the jump in $\rho(T)$ at T_{SDW} and the opening of an optical gap below. Although the overall spectral weight is eventually conserved, a considerable fraction (as discussed in Sec. IV B) is shifted to energies above the gap. Accordingly a reduced $\omega_p^*(T)$ should be used for the generalized Drude analysis in Eq. (3) for 170, 100, and 10 K: $\omega_p^*/(2\pi c)\approx 12$ 900, 11 900 and 11 000 cm^{-1}, respectively. The enhancement of the effective mass extends over a wide energy range and amounts up to $m^*/m_b\approx 21$ for $T=10$ K as displayed in Fig. 7(c).[41]

For $T<T_{SDW}$, $1/\tau(\omega)$ is strongly suppressed at low frequencies due to reduced phase space for scattering of charge carriers upon opening of the SDW gap. This result agrees with dc resistivity (cf. Sec. III A) where we concluded that the slope of $\rho(T)$ gets steeper due to the same effect. We find a linear increase in $1/\tau(\omega)$ up to approximately 200 cm^{-1}, as

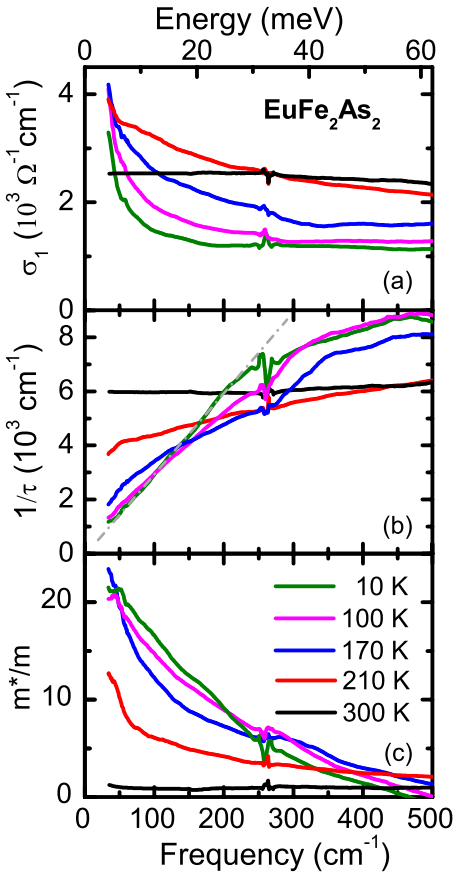

FIG. 7. (Color online) (a) In-plane conductivity of $EuFe_2As_2$ in the far-infrared spectral range. (b) Frequency-dependent scattering rate and (c) frequency-dependent effective mass as obtained from an extended Drude analysis of the optical spectra. The dashed line in panel (b) indicates the linear behavior of $1/\tau(\omega)$.

seen from Fig. 7(b). This evidences scattering on bosonic excitations, for instance, excitations of the spin-density wave.[42] The slope grows as the temperature decreases because the magnetic order is completed further. The AFM ordering of the Eu^{2+} ions at T_N has little influence on the electronic scattering processes in this energy range and seems to be confined to the in-plane dc transport, which is not surprising since $\hbar\omega > k_B T_N$. Below 500 cm^{-1}, the effective mass also starts to increase and m^*/m_b reaches more than 20 below T_{SDW}, indicating that the carriers are strongly interacting.

Here one should note that in the frequency range of our extended Drude analysis, the conductivity is dominated by the response of mobile carriers. In Fig. 7(c) we can see that at m^* becomes negative at approximately 470 cm^{-1}. This is a clear sign that the data above 470 cm^{-1} are dominated by density-of-states effects such as energy gaps or interband transitions; an interpretation in terms of scattering rate and effective mass becomes meaningless.[42] Hence, to make sure that the SDW gap does not mislead our analysis of the carrier dynamics in terms of $1/\tau(\omega)$ and $m^*(\omega)$, we also extracted all the high-frequency features, leaving only the zero-frequency contributions for an extended Drude analysis. The results obtained this way remain the same in the low-frequency range as plotted in Fig. 7; this strongly supports,

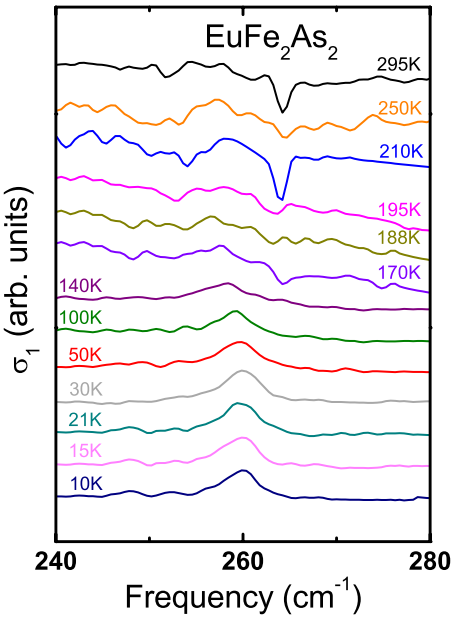

FIG. 8. (Color online) Temperature development of the conductivity in the region of the phonon mode of $EuFe_2As_2$. The different spectra are displaced for clarity reasons.

that our analysis procedure and interpretation is valid and robust.

It is instructive to compare our findings with the spectra of chromium, the canonical example of a three-dimensional SDW system.[40,43,44] There also a gap opens over some parts of the Fermi surface as a consequence of the SDW ordering. Below T_{SDW} the Drude mode narrows and the low-energy spectral weight is suppressed. From the extended Drude analysis a suppression of the scattering rate in the SDW state was obtained below 500 cm^{-1} and an overshoot for higher frequencies. Basov *et al.* argued that the area above and below the SDW transition should be conserved.[44] Indeed, this is true if we consider $1/\tau(\omega)$ in the whole frequency range. However, the most important part of our extended Drude analysis is confined to the narrow Drude response (not analyzed for Cr). Similar to the case of Cr, this contribution becomes sharper for $T < T_{SDW}$ due to the reduced phase space, described by a drop in $1/\tau(\omega)$. The information is obtained from the particular shape of the zero-frequency response and its temperature dependence.

Yang *et al.* performed an extended Drude analysis of their optical spectra on $Ba_{0.55}K_{0.45}Fe_2As_2$ after subtracting the mid-infrared contribution described by a Lorentz oscillator.[39] The low-temperature scattering rate increases with frequency for $\omega/(2\pi c) < 400$ cm^{-1}, which was interpreted as bosonic excitations—most probable magnetic fluctuations—in support of our findings.

E. Vibrational features

In our optical spectra displayed in Fig. 6(a), a phonon mode at 260 cm^{-1} is clearly observed for all the temperatures. This E_u mode involves the displacements of the Fe and As ions and is of particular importance because it changes its

TABLE I. Transport and optical parameters of $EuFe_2As_2$ as obtained from our investigations on single crystals. ρ_{ab} and ρ_c denote the room-temperature resistivity. ω_p is the plasma frequency within the highly conducting plane, from which the carrier density n and the bandmass m_b is obtained. From the room-temperature scattering rate $1/\tau$, the mean free path ℓ is evaluated, assuming a Fermi velocity of $v_F=2\times10^6$ m/s [typical for metals (Ref. 49)]. 2Δ is the value of the zero-temperature SDW gap. T_{SDW} and T_N refer to the ordering temperatures of the SDW and AFM phase, respectively. At $T=10$ K the effective mass related to the zero-frequency contribution is enhanced by m^*/m_b.

ρ_{ab} (m Ω cm)	ρ_c (m Ω cm)	$\omega_p/(2\pi c)$ (cm^{-1})	n (cm^{-3})	m_b m_0	$1/\tau$ (s^{-1})	ℓ (nm)	2Δ (cm^{-1})	T_{SDW} (K)	T_N (K)	m^* m_b
0.41	3.0	13800	4.2×10^{21}	2	1.8×10^{14}	11	750	189	19	21

shape and position upon cooling. In Fig. 8 we magnify this spectral region and plot the conductivity for various temperatures. For $T\geq170$ K, this phonon appears at 264.2 cm^{-1} as an antiresonance. It can be followed down to $T=210$ K and then becomes more and more obscured as T decreases; below 170 K the antiresonance feature is basically absent. Instead a normal phonon mode develops at lower frequency 257 cm^{-1}, which as a matter of fact can be identified all the way up to 190 K. The mode becomes stronger upon cooling down to $T=10$ K and hardens to 260 cm^{-1}.

The antiresonance can be successfully fitted applying Fano's theory:[45,46]

$$\sigma_1(\omega)=i\sigma_0(q-i)^2(i+x)^{-1}, \tag{5}$$

where σ_0 is the background, $x=(\omega^2-\omega_T^2)/\gamma\omega$ (γ and ω_T are the linewidth and the resonant frequency, respectively), and q is the Fano parameter reflecting the degree of asymmetry of the peak. The best description we get is $\omega_T=263.4$ cm^{-1} and $q=-0.17$ for high temperatures. Such a low and negative value of q indicates the single level for vibration is overlapping with the electronic background which is interacted.[46] For $T<170$ K, the fit yields $|q|\rightarrow\infty$ and the Lorentz line shape is recovered, indicating a noninteracting case appears upon the SDW gap opening. In conclusion, no new phonon appears due to the structural phase transition, but the significant modification of the vibrational feature around 260 cm^{-1} upon cooling is caused by the change in the electronic background to which it is coupled. The coexistence of reminiscent features of both limiting cases—the mode and the antimode—in such a wide temperature range implies either strong fluctuation effects or inhomogeneities or phase separation in the vicinity of the SDW transition.

The shape variation of this phonon mode by crossing the SDW transition implies that the Fe electrons interacting with this phonon are condensed to the gap feature. Our finding corresponds to the conclusions from Raman scattering experiments on $CaFe_2As_2$ and $SrFe_2As_2$,[47] which suggest the variation in the phonon parameters is mainly caused by the change in charge distribution within the FeAs plane and accordingly the strength of the electron-phonon interaction. In the latest report of first-principles calculations for $CaFe_2As_2$, it is also suggested that modifying the chemistry of the Fe ion due to the decrease in Fe moment will decrease the Fe-As interaction.[48]

V. CONCLUSIONS

The magnetic, transport, and optical properties of $EuFe_2As_2$ single crystals have been investigated parallel and perpendicular the highly conducting *ab* plane. In Table I we summarize the parameters obtained. The anisotropy $\rho_c/\rho_{ab}\approx8$ is basically temperature independent. From our optical data the carrier density was estimated to 4.2×10^{21} cm^{-3} and the bandmass $m_b=2m_0$. The magnetic susceptibility is solely determined by the localized magnetic moments of the Eu^{2+} ions with only little interaction to the Fe subsystem. The charge-carrier dynamics of $EuFe_2As_2$, on the other hand, is strongly affected by the spin-density-wave transition at $T_{SDW}=189$ K when a gap opens in the optical spectrum around 1000 cm^{-1}. A modification of the Fe-As lattice vibration upon opening of the SDW gap reflects an interaction with the electronic background that gets much less pronounced in the SDW state. The remaining charge carriers are strongly influenced by scattering at spin fluctuations that can be modified by an external magnetic field. The extended Drude analysis gives a linear dependence of the scattering rate with frequencies at low temperatures. The effective mass m^*/m_b enhances by a factor of 21 at $T=10$ K. Both parameters evidence the interaction of the low-energy charge carriers with SDW excitations.

ACKNOWLEDGMENTS

We thank J. Braun for ellipsometric measurements in the visible range. We acknowledge help of and discussions with B. Gorshunov and V. I. Torgashev. This work was partially supported by the Deutsche Forschungsgemeinschaft (DFG). N.B. acknowledges support from the Alexander von Humboldt Foundation. N.D. is grateful for the support by the Magarete-von-Wrangell Programm of Baden-Württemberg. The work at Zhejiang University was supported by NSF of China.

*dan.wu@pi1.physik.uni-stuttgart.de

[1] H. R. Ott, Prog. Low Temp. Phys. **11**, 215 (1987); N. Grewe and F. Steglich, *Handbook on the Physics and Chemistry of Rare Earths*, edited by K. A. Gscheidner, Jr. and L. Eyring (Elsevier, Amsterdam, 1991), Vol. 14, p. 343.

[2] T. Ishiguro, K. Yamaji, and G. Saito, *Organic Superconductors*, 2nd ed. (Springer-Verlag, Berlin, 1998).

[3] N. Ichikawa, S. Uchida, J. M. Tranquada, T. Niemöller, P. M. Gehring, S.-H. Lee, and J. R. Schneider, Phys. Rev. Lett. **85**, 1738 (2000).

[4] Y. Kamihara, T. Watanabe, M. Hirano, and H. Hosono, J. Am. Chem. Soc. **130**, 3296 (2008).

[5] X. H. Chen, T. Wu, G. Wu, R. H. Liu, H. Chen, and D. F. Fang, Nature (London) **453**, 761 (2008).

[6] G.-F. Chen, Z. Li, W. Z. Hu, J. Dong, X. D. Zhang, P. Zheng, N. L. Wang, and J. L. Luo, Chin. Phys. Lett. **25**, 3403 (2008).

[7] M. Rotter, M. Tegel, D. Johrendt, I. Schellenberg, W. Hermes, and R. Pottgen, Phys. Rev. B **78**, 020503(R) (2008); Phys. Rev. Lett. **101**, 107006 (2008); M. Rotter, M. Tegel, I. Schellenberg, F. M. Schappacher, R. Pöttgen, J. Deisenhofer, A. Günther, F. Schrettle, A. Loidl, and D. Johrendt, New J. Phys. **11**, 025014 (2009).

[8] D. Kasinathan, A. Ormeci, K. Koch, U. Burkhardt, W. Schnelle, A. Leithe-Jasper, and H. Rosner, New J. Phys. **11**, 025023 (2009).

[9] H. Raffius, M. Mörsen, B. D. Mosel, W. Müller-Warmuth, W. Jeitschko, L. Terbüchte, and T. Vomhof, J. Phys. Chem. Solids **54**, 135 (1993).

[10] S. Jiang, Y. K. Luo, Z. Ren, Z. W. Zhu, C. Wang, X. F. Xu, Q. Tao, G. H. Cao, and Z.-A. Xu, New J. Phys. **11**, 025007 (2009).

[11] A. S. Sefat, R. Y. Jin, M. A. McGuire, B. C. Sales, D. J. Singh, and D. Mandrus, Phys. Rev. Lett. **101**, 117004 (2008).

[12] L. J. Li, Y. K. Luo, Q. B. Wang, H. Chen, Z. Ren, Q. Tao, Y. K. Li, X. Lin, M. He, Z. W. Zhu, G. H. Cao, and Z.-A. Xu, New J. Phys. **11**, 025008 (2009).

[13] Z. Ren, X. Lin, Q. Tao, S. Jiang, Z. Zhu, C. Wang, G. Cao, and Z.-A. Xu, arXiv:0810.2595, Phys. Rev. B (to be published).

[14] H. S. Jeevan, Z. Hossain, D. Kasinathan, H. Rosner, C. Geibel, and P. Gegenwart, Phys. Rev. B **78**, 092406 (2008).

[15] V. A. Gasparov, H. S. Jeevan, and P. Gegenwart, arXiv:0902.2190 (unpublished).

[16] C. F. Miclea, M. Nicklas, H. S. Jeevan, D. Kasinathan, Z. Hossain, H. Rosner, P. Gegenwart, C. Geibel, and F. Steglich, arXiv:0808.2026 (unpublished).

[17] Z. Ren, Q. Tao, S. Jiang, C. Feng, C. Wang, J. Dai, G. Cao, and Z.-A. Xu, arXiv:0811.2390, Phys. Rev. Lett. (to be published).

[18] J. Dai, Q. Si, J. X. Zhu, and E. Abrahams, Proc. Natl. Acad. Sci. U.S.A. **106**, 4118 (2009).

[19] From our measurements of a number of crystals from different sources, the exact shape of $\rho_c(T)$ is sample dependent at low temperature. For instance, the hump around 70 K shows up in different strengths depending on the crystal. We also found that samples like to cleave in flakes which might infer a larger out-of-plane resistivity than intrinsically present. Besides, we notice that there is another report of the $\rho_c(T)$ of $EuFe_2As_2$ (Ref. 31), and the bump is absent in their results.

[20] We use *ab* plane throughout this paper; it is identical with the basal plane (in-plane) of the tetragonal crystal structure where $a=b$.

[21] M. Dressel and G. Grüner, *Electrodynamics of Solids* (Cambridge University Press, Cambridge, 2002).

[22] H. S. Jeevan, Z. Hossain, D. Kasinathan, H. Rosner, C. Geibel, and P. Gegenwart, Phys. Rev. B **78**, 052502 (2008).

[23] D. J. Singh, Phys. Rev. B **78**, 094511 (2008).

[24] F. J. Ma, Z. Y. Lu, and T. Xiang, arXiv:0806.3526 (unpublished).

[25] T. Yildirim, Phys. Rev. Lett. **102**, 037003 (2009).

[26] N. F. Mott, Proc. R. Soc. Lond. **156**, 368 (1936); N. F. Mott, Adv. Phys. **13**, 325 (1964); I. A. Campbell and A. Fert, *Ferromagnetic Materials*, edited by E. P. Wohlfarth (North-Holland, Amsterdam, 1982), Vol. 3, p. 747; J. M. Fournier and E. Gratz, *Handbook on the Physics and Chemistry of Rare Earths*, edited by K. A. Gschneidner, L. Eyring, H. G. Lander, and G. R. Choppin (North-Holland, Amsterdam, 1993), Vol. 17, p. 409.

[27] M. V. Sadovskii, Phys. Usp. **51**, 1201 (2008).

[28] M. M. Altarawneh, K. Collar, C. H. Mielke, N. Ni, S. L. Budko, and P. C. Canfield, Phys. Rev. B **78**, 220505(R) (2008).

[29] H. Q. Yuan, J. Singleton, F. F. Balakirev, S. A. Baily, G. F. Chen, J. L. Luo, and N. L. Wang, Nature (London) **457**, 565 (2009).

[30] X. F. Wang, T. Wu, G. Wu, H. Chen, Y. L. Xie, J. J. Ying, Y. J. Yan, R. H. Liu, and X. H. Chen, Phys. Rev. Lett. **102**, 117005 (2009).

[31] T. Wu, G. Wu, H. Chen, Y. L. Xie, R. H. Liu, X. F. Wang, and X. H. Chen, arXiv:0808.2247 (unpublished).

[32] D. N. Basov and T. Timusk, Rev. Mod. Phys. **77**, 721 (2005).

[33] M. Dressel and N. Drichko, Chem. Rev. **104**, 5689 (2004).

[34] W. Z. Hu, J. Dong, G. Li, Z. Li, P. Zheng, G. F. Chen, J. L. Luo, and N. L. Wang, Phys. Rev. Lett. **101**, 257005 (2008).

[35] F. Pfuner, J. G. Analytis, J.-H. Chu, I. R. Fisher, and L. Degiorgi, Eur. Phys. J. B **67**, 513 (2009).

[36] M. Tegel, M. Rotter, V. Weiss, F. M. Schappacher, R. Poettgen, and D. Johrendt, J. Phys.: Condens. Matter **20**, 452201 (2008).

[37] This obvious discrepancy can only be explained by differences in sample quality. In our case of $EuFe_2As_2$ the optical results on several crystals of different origin consistently show only one clear-cut gap around 1000 cm^{-1}.

[38] A. B. Kuzmenko, F. P. Mena, H. J. A. Molegraaf, D. van der Marel, B. Gorshunov, M. Dressel, I. I. Mazin, J. Kortus, O. V. Dolgov, T. Muranaka, and J. Akimitsu, Solid State Commun. **121**, 479 (2002).

[39] J. Yang, D. Hüvonen, U. Nagel, T. Rõõm, N. Ni, P. C. Canfield, S. L. Bud'ko, J. P. Carbotte, and T. Timusk, arXiv:0807.1040 (unpublished).

[40] S. V. Dordevic and D. N. Basov, Ann. Phys. **15**, 545 (2006).

[41] Alternatively, we could consider only the zero-frequency contribution, which has been modeled by the Drude term in Fig. 6 and led to the zero crossing of $\epsilon_1(\omega)$ around 500 cm^{-1}. In that case the low plasma frequency $\omega_{p,D}/2\pi c \approx 3400$ cm^{-1} yields a zero-frequency effective mass of only $m_D^*/m=4$. The latter approach, however, seems to be inappropriate because it accounts only for the excitations below 100 cm^{-1} but does not describe the far-infrared behavior in its full extent.

[42] A. J. Millis, A. Zimmers, R. P. S. M. Lobo, N. Bontemps, and C. C. Homes, Phys. Rev. B **72**, 224517 (2005).

[43] A. S. Barker, B. I. Halperin, and T. M. Rice, Phys. Rev. Lett. **20**, 384 (1968).

[44] D. N. Basov, E. J. Singley, and S. V. Dordevic, Phys. Rev. B **65**, 054516 (2002).

[45] U. Fano, Phys. Rev. **124**, 1866 (1961).

[46] A. Damascelli, K. Schulte, D. van der Marel, and A. A. Menovsky, Phys. Rev. B **55**, R4863 (1997).
[47] K. Y. Choi, D. Wulferding, P. Lemmens, N. Ni, S. L. Bud'ko, and P. C. Canfield, Phys. Rev. B **78**, 212503 (2008); G. L. Sun, D. L. Sun, M. Konuma, P. Popovich, A. Boris, J. B. Peng, K.-Y. Choi, P. Lemmens, and C. T. Lin, arXiv:0901.2728 (unpublished).
[48] T. Yildirim, Phys. Rev. Lett. **102**, 037003 (2009).
[49] C. Kittel, *Introduction to Solid State Physics*, 8th ed. (Wiley, New York, 2005).